ABSTRACT

CLOSE-IN AIRBLAST FROM UNDERGROUND EXPLOSIONS

Air overpressures as a function of time have been measured from surface zero to about 170 ft/lb$^{1/3}$ along the ground from nuclear and chemical explosions. Charge depths varied from the surface to depths below which explosion gases are contained. A ground-shock-induced air pressure pulse is clearly distinguishable from the pulse caused by venting gases. Measured peak overpressures show reasonable agreement with the theoretical treatment by Montan.* In a given medium the suppression of blast with explosion burial depth is a function of the relative distance at which the blast is observed. Rates of suppression of peak overpressure with charge burial are different for the two pulses. Rates are determined for each pulse over the range of distances at which measurements have been made of air overpressure from chemical explosions in several media. Nuclear data are available from too few shots for similar dependence on burial depth and distance to be developed, but it is clear that the gas venting peak overpressure from nuclear explosions is much more dependent on medium than that from chemical explosions.

For above-ground explosions, experiment has shown that airblast from a 1-kiloton nuclear explosion is equal to that from a 0.5-kiloton TNT explosion. Data on ground-shock-induced airblast is now sufficient to show that a similar relationship may exist for buried explosions. Because of medium dependence of the gas venting pulse from nuclear explosions, data from additional nuclear events will be required before a chemical/nuclear airblast equivalence can be determined for the gas-venting pulse.

---

*D. H. Montan, "Source of Airblast from an Underground Explosion," Transactions, American Nuclear Society, Vol. II, No. 2, November 1968, pp. 541, 542.

CLOSE-IN AIRBLAST FROM UNDERGROUND EXPLOSIONS

L. J. Vortman
Sandia Laboratories
Albuquerque, New Mexico

INTRODUCTION AND BACKGROUND

Airblast has been measured near the ground surface close to a large number of cratering detonations of buried chemical explosives in single-charge (Table 1), row-charge (Table 2), and horizontal-array (Table 3) configurations. The term "close-in" refers to distances sufficiently small that meteorological effects on blast propagation are not significant. Measurements have been made on a smaller number of detonations of single-charge nuclear explosions and on one row-charge nuclear explosion at charge burial depths at which craters are formed (Table 4), and on several single-charge nuclear explosions at charge burial depths great enough to contain explosion products (Table 5). Airblast is a function of the medium surrounding the explosion, explosion energy, type of explosive, charge burial depth, and distance from the epicenter; these parameters are included in the tables.

It is useful to identify principal characteristics of a typical overpressure-time history (Figure 1) for an explosion buried near the depth which produces maximum crater dimensions and to associate those characteristics with mechanisms causing them. The two major characteristics are the ground-shock-induced (GSI) pulse and the pulse from venting gases.

Neglecting gravity and layering effects, ground shock propagates essentially spherically until the surface is reached, and free-field ground particle velocity (u) can be defined by

$$u = c\ (R/W^{1/3})^{-\beta} \qquad (1)$$

where R is the radial distance in the ground, W is the explosion energy, and c and β are medium dependent. Particle velocity in the ground can be determined from hydrodynamic calculations or, since such calculations are not readily available, and tend to decrease in accuracy with increased R, ground particle velocities determined experimentally[32] for several media may be used. The vertical component of free-surface particle velocity (u_{vfs}) at the

TABLE 1

HE Single Charges

Shot or Series	Date	Soil Type	Charge Weight[a] (lb)	Number of Shots	Range of Charge Burial Depth		Range of Distance Over Which Airblast was Measured		Ref
					Actual (ft)	Scaled ($ft/lb^{1/3}$)	Actual (ft)	Scaled ($ft/lb^{1/3}$)	
UET-312	05/05/51	Dry Clay	2560	1	7	0.5	41-180	3.0-13.0	1
UET-315	05/10/51	Dry Clay	40,000	1	17	0.5	102.5-450	3.0-13	1
UET-318	05/22/51	Dry Clay	320,000	1	35	0.5	205-1230	3-18	1
Jangle HE 1, 3	08/25/51-09/15/51	Alluvium NTS	2560	2	1.9-6.9	0.15-0.5	28.4-1025	2.08-75	2
Jangle HE 2	09/03/51	Alluvium NTS	40,000	1	4.7	0.15	85.5-1025	2.49-30	2
Mole 100 Series	08/28/52-07/19/52	Dry Clay	256	4	1.6-6.4	0.26-1.0	12-80	1.89-12.6	3
Mole 200 Series	09/14/52-10/24/52	Alluvium NTS	256	5	0.8-6.4	0.13-1.00	12-80	1.89-12.6	3
Mole 300-309 Series	09/15/53-10/16/53	Wet Sand	256	6	0.8-4.8	0.13-0.75	15-80	2.36-12.6	3
Mole 311	10/20/53	Moist Clay	256	1	3.2	0.50	20-80	3.16-12.6	3
Mole 400 Series	10/23/54-11/04/54	Alluvium NTS	256	6	0.8-6.4	0.13-1.00	15-60	2.36-9.46	3
Sandia I Series	01/21/59-01/27/59	Alluvium NTS	256	7	6.4-19.0	1.0-3.0	60, 80	9.46, 12.6	4
Area 14 Series	04/10/59-04/21/59	Tuff NTS	256	9	6.9-18.7	1.09-2.94	25.5	4.02	5
Stagecoach 1, 2, 3	03/15/60-03/25/60	Alluvium NTS	40,000	3	17.1, 34.6, 80	0.5, 1.0, 2.3	80-5020	2.34-146.8	6
Buckboard 11, 12, 13	08/24/60-09/27/60	Basalt	40,000	3	25.5, 42.7, 58.8	0.75, 1.25, 1.72	59.5-480	1.74-14.0	7
Scooter	10/13/60	Alluvium NTS	987,410	1[e]	125	1.25	300-6500	3-25	8
TTR-211-4, 5	05/22/64-05/26/64	Playa	64	2	5.5, 6.0	1.36, 1.50	50-1500	12.5-375	9, 10
TTR-211-6, 7, 8	06/01/64-06/18/64	Playa	700	3	6, 13	0.68, 1.50	50-1500	12.5-375	10
Sandia III (pre Capsa) 1 and 2	05/03/65-05/06/65	Alluvium ABQ	256	2[e]	9.5	1.50	50, 150	7.85-23.6	10
Pre-Schooner II	09/30/65	Rhyolite	189,200[b]	1[e]	71	1.24	0-4000	0-69.7	11
Capsa 1-8	08/16/66-09/13/66	Alluvium ABQ	1000	8[e]	10, 12.5, 15, 17.5	1, 1.25, 1.5, 1.75	0-700	0-70	10
TTR-211-42	10/25/66	Playa	64	1	6.9	1.73	50-1500	12.5-375	9
Capsa 9	05/21/68	Alluvium ABQ	1000	1[e]	12.5	1.25	0-700	0-70	10
Capsa 10	05/29/68	Alluvium ABQ	1000[b]	1[e]	12.5	1.25	0-700	0-70	10
Capsa 11	10/13/68	Alluvium ABQ	30,478[c]	1[e]	47.9	1.53	0-2275	0-73	10
Capsa 12-13	07/25/68	Alluvium ABQ	979[b]	2[e]	12.5, 15.0	1.25, 1.50	0-200	0-70	10
Tugboat 1a, b, c, d	11/04/69-11/06/69	Water-Covered Coral	2000[d]	4	17.33, 17.86, 21.72, 25.84	1.38, 1.42, 1.72, 2.05	259-8425	20.6-669	12
Tugboat 1e	11/07/69	Water-Covered Coral	20,000[d]	1	42.9	1.58	277-8614	10.2-317	12

[a] TNT unless otherwise noted

[b] Nitromethane

[c] Composition B

[d] Aluminized ammonium nitrate

[e] Measurements were also made at airborne stations well above ground level

TABLE 2

HE Row Charges

Shot or Series	Date	Soil Type	Charge Weight[a] (lb)	Number of Shots	Number of Charges in Each Row	Charge Burial Depth		Spacing Between Charges		Range of Distance Over Which Airblast was Measured[b]		Reference
						Actual (ft)	Scaled (ft/lb$^{1/3}$)	Actual (ft)	Scaled (ft/lb$^{1/3}$)	Actual (ft)	Scaled (ft/lb$^{1/3}$)	
Dugout	6/24/64	Basalt	40,000[c]	1	5	58.8	1.72	45	1.31	170 - 5000	4.97 - 146	13
Pre-Capsa 3	5/27/65	Alluvium (Abq)	256	1[d]	5	9.5	1.50	13.6	2.14	75 - 600	11.8 - 94.5	10
TTR-211-41	10/5/66	Playa	64	1	2	6	1.50	8	2	50 - 1500	12.5 - 375	9
TTR-211-44	11/22/66	Playa	64	1	5	6	1.50	8	2	50 - 1500	12.5 - 375	9
TTR-211-10,13	8/20/64 3/3/65	Playa	64	2	11	6	1.50	8	2	50 - 1500[e]	12.5 - 375	9
TTR-211-43	11/18/66	Playa	64	1	25	6	1.50	8	2	50 - 1500	12.5 - 375	9
TTR-211-46	3/27/67	Playa	64	1	2	6.9	1.73	5.25	1.31	50 - 1500	12.5 - 375	9
TTR-211-16	5/27/65	Playa	64	1	5	6.9	1.73	5.25	1.31	19.9 - 567	5 - 142	9, 14
TTR-211-45	2/24/67	Playa	64	1	11	6.9	1.73	5.25	1.31	50 - 1500	12.5 - 375	9
Pre-Gondola II	6/28/67	Shale	E 77,200[c]			59.7	1.40	105.5	2.48	225 - 5000	5.3 - 117	15
			F 39,400[c]			49.4	1.45	79.8	2.35	225 - 5000	6.6 - 147	--
			G 39,100[c]	1	5	48.8	1.44	79.9	2.88	225 - 5000	6.6 - 147	--
			H 79,120[c]			59.9	1.40	79.9	1.86	225 - 5000	5.2 - 116	--
			I 40,000[c]			48.8	1.43	79.9	2.34	225 - 5000	6.6 - 146	--

[a] TNT unless otherwise noted

[b] Measurements made perpendicular to and off end of row

[c] Nitromethane

[d] Measurements were also made at airborne stations above ground

[e] Measurements were also made on line 45 degrees radially from end charges

TABLE 3

ARRAYS OF CHARGES

Shot or Series	Date	Soil Type	Charge Weight[a]	Number of Charges	Charge Burial Depth		Spacing Between Charges		Range of Distance Over Which Airblast was Measured		Reference
					Actual (ft)	Scaled ($ft/lb^{1/3}$)	Actual (ft)	Scaled ($ft/lb^{1/3}$)	Actual (ft)	Scaled ($ft/lb^{1/3}$)	
Quincuncial Arrays (Five Charge Square)[b]											
TTR-211-22	8/26/65	Playa	64	5	6	1.5	10	2.5	50 - 1500	12.5 - 375	16
TTR-211-27	9/9/65	Playa	64	5	8	2	10	2.5	50 - 1500	12.5 - 375	16
TTR-211-28	9/10/65	Playa	64	5	10	2.5	10	2.5	50 - 1500	12.5 - 375	16
TTR-211-35	11/8/65	Playa	64	5	6	1.5	16	4	50 - 1500	12.5 - 375	16
TTR-211-32	11/9/65	Playa	64	5	8	2	16	4	50 - 1500	12.5 - 375	16
TTR-211-29	9/27/65	Playa	64	5	10	2.5	16	4	50 - 1500	12.5 - 375	16
Double Row (118.8 feet between rows)											
Pre-Gondola III, Phase I		Shale	2000[c]	14	19.5	1.55	27	2.14	93 - 320	7.38 - 254	17

[a] TNT unless otherwise noted

[b] Measurements made perpendicular to one side of square

[c] Nitromethane

TABLE 4

Nuclear Cratering Shots

Shot or Series	Date	Soil Type	Yield (kt)	Charge Burial Depth			Range of Distance Over Which Airblast was Measured			Reference
				Actual (ft)	Scaled ($ft/kt^{1/3}$)	Scaled ($ft/lb^{1/3}$)	Actual (ft)	Scaled ($ft/kt^{1/3}$)	Scaled ($ft/lb^{1/3}$)	
Jangle U	11/29/51	Alluvium (NTS)	1.2	17	16	0.13[a]	314 - 3,100	295 - 2,917	2.35 - 31.4	18
Teapot ESS	3/23/55	Alluvium (NTS)	1.2	67	63	0.50	250 - 600	235 - 565	1.86 - 4.48	19
Danny Boy	3/5/62	Basalt	0.43	110	146	1.16	200 - 8,500	265 - 11,261	2.12 - 90.1	20
Sedan	7/6/62	Alluvium (NTS)	100	635	137	1.09	2,960 - 15,500	638 - 3,339	5.06 - 26.5	21
Johnie Boy	7/11/62	Alluvium (NTS)	0.5	2	2.5	0.02	65 - 16,126	82 - 20,317	0.65 - 161.3	22
Sulky	12/18/64	Basalt	0.085	90	205	1.62	165 - 3,772	375 - 8,579	6.77 - 155	23
Palanquin	4/14/65	Rhyolite	4.3	280	172	1.36	21 - 7,380	12.9 - 4,538	0.1 - 36	24
Cabriolet	1/26/68	Rhyolite	2.3	171	130	1.03	3.35 - 6,000	2.5 - 4,545	0 - 36.1	25
Buggy I[b]	3/12/68	Basalt	Five 1.1	135	131	1.04	500 - 10,500[c]	484 - 10,172	3.8 - 81	26
Schooner	12/8/68	Rhyolite	31	355	113	0.90	21 - 15,600	6.7 - 4,966	0 - 39.4	27

[a]Measurements were also made at airborne stations above ground

[b]Row charge spacing between charges 150 feet

[c]Measurements made along four lines--two perpendicular to midpoint of rows, two off the ends of the row

TABLE 5

Nuclear Contained Shots

Shot or Series	Date	Soil Type	Yield (kt)	Charge Burial Depth			Distance at Which Airblast was Measured			Reference
				Actual (ft)	Scaled ($ft/kt^{1/3}$)	Scaled ($ft/lb^{1/3}$)	Actual (ft)	Scaled ($ft/kt^{1/3}$)	Scaled ($ft/lb^{1/3}$)	
Gnome	12/10/61	Halite	3	1184	821	6.52	40, 1,000, 2,500	28, 693, 1733	122, 5.5, 13.8	28
Dumont	5/19/66	Tuff	a	2201	a	a	0, 3,000, 6,000, 14,000, 30,000	a	a	10
Greeley	12/20/66	Saturated tuff	825	3991	426	3.38	50, 2,000, 4,000, 16,487, 32,853, 65,788	5.3, 213, 426, 1758, 3503, 7014	0.04, 1.69, 3.39, 14.0, 27.8, 55.7	10
Scotch	5/23/67	Tuff	150	3210	604	4.80	71, 7,515, 19,890	13.4, 1414, 3743	0.1, 11.2, 29.7	29
Faultless	1/19/68	Tuff	a	3200	a	a	1,500, 6,000	a	a	10
Boxcar	4/26/68	Rhyolite	1200	3822	360	2.85	75, 1,000, 11,504	7.1, 94, 1083	0.06, 2.75, 8.59	29, 30
Milrow	10/2/69	Pillow lava	about 1000	3992	~39.9	3.17	300, 4,000	~30, ~400	~0.24, ~3.17	10, 32

[a]Yield is classified

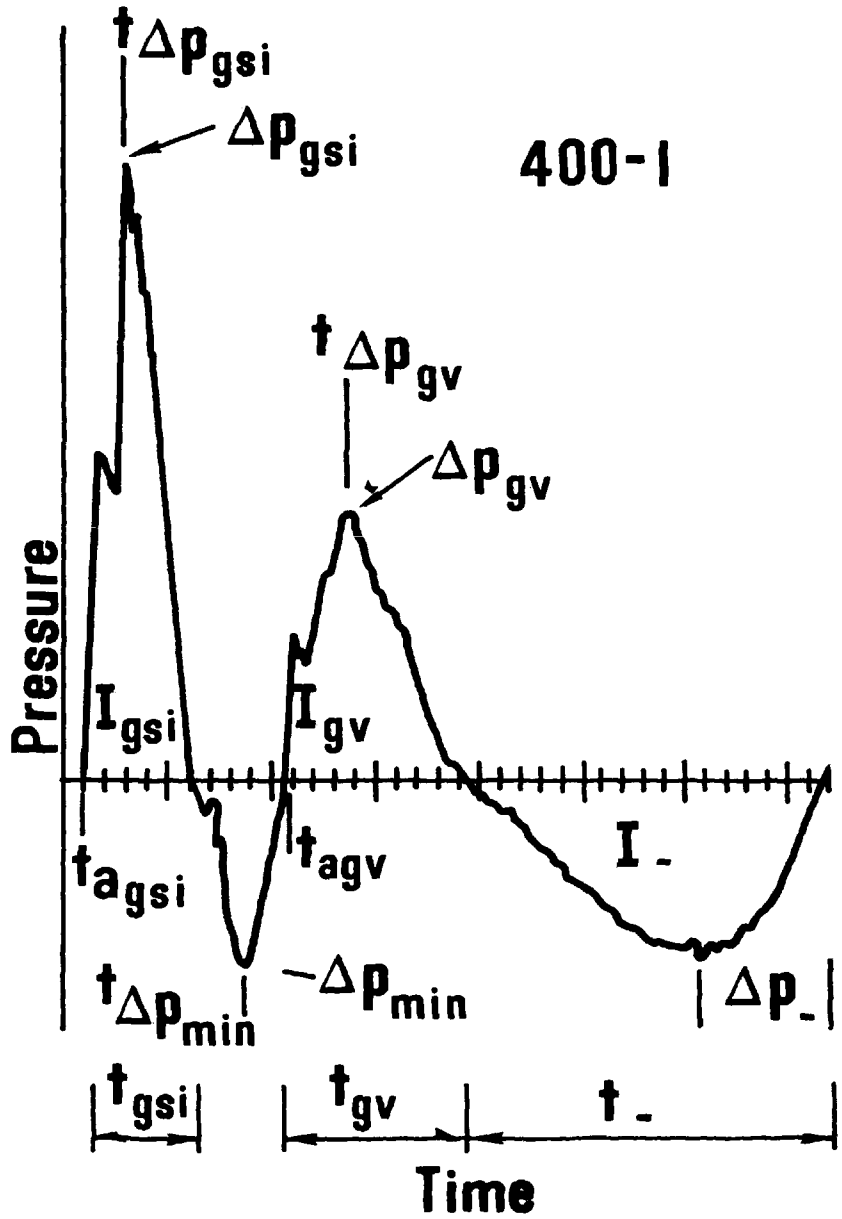

Δp_{gsi} = peak positive overpressure of ground-shock-induced pulse

Δp_{min} = minimum pressure between pulses; may be positive or negative

Δp_{gv} = peak positive overpressure of venting gas pulse

Δp_- = peak negative pressure

I_{gsi} = positive impulse of ground shock pulse

I_{gv} = positive impulse of venting gas pulse

I_+ = total positive impulse: $I_{gsi} + I_{gv}$

I_- = negative impulse

$t_{a_{gsi}}$ = time of arrival of ground-shock-induced pulse

$t_{a_{gv}}$ = time of arrival of gas venting pulse; may coincide with $t_{\Delta p_{min}}$

$t_{\Delta p_{gsi}}$ = time of peak positive overpressure of ground-shock-induced pulse

$t_{\Delta p_{min}}$ = time of minimum pressure between pulses

$t_{\Delta p_{gv}}$ = time of peak positive overpressure of gas venting pulse

t_{gsi} = duration of ground-shock-induced pulse

t_{gv} = duration of gas venting pulse

t_+ = duration of positive phase = $t_{gsi} + t_{gv}$

t_- = duration of negative phase

Fig. 1—Typical airblast waveform for buried explosions.

air-ground interface at a horizontal distance (r) from the epicenter, is

$$u_{vfs} = 2u \left(\frac{DOB}{R}\right) \qquad (2)$$

where DOB is the depth-of-burst to the charge center and r is $(R^2 - DOB^2)^{1/2}$. Where the air overpressure is induced at r by u_{vfs} and where r is also the point of observation or measurement, the overpressure pulse is defined here as a ground-transmitted GSI pulse, and can be identified by an arrival time associated with ground shock propagation velocity; e.g., the first peak overpressure in Figure 1. Where the horizontal distance to the point of observation or measurement is greater than the distance, r, at which the overpressure is induced, the arrival of the pulse is delayed by the slower propagation velocity in air from r to the point of observation. That pulse is defined here as the air-transmitted GSI pulse; e.g., the maximum peak in Figure 1. This pulse has an apparent source along the surface away from the epicenter. The ground-transmitted GSI pulse attenuates rapidly and is rarely observed at r > 3 DOB because gages ordinarily are set to measure the larger air-transmitted GSI pulse.

At relatively large horizontal distances, a train of minor pulses can be observed in some media preceding the air-transmitted GSI pulse. The train is induced by the vertical component of ground motion of either surface waves, refracted body waves, or a combination of both.

The gas-venting pulse is the second major characteristic of the overpressure waveform from buried explosions. The overpressure transferred to the atmosphere is a function of the gas cavity volume and pressure at the time venting occurs, which are, in turn, dependent on burial depth, medium, and type of explosive. Sedan[21], a nuclear detonation in alluvium, vented while the cavity was under high pressure, producing a relatively high overpressure, whereas cavities of Pre-Gondola II[15] and Pre-Gondola III, Phase I[17] (nitromethane detonations in shale) continued to expand until cavity pressure approached ambient, producing a gas-venting pulse that was barely identifiable.

There is one other contribution to the overpressure waveform. From the time of arrival of the ground shock at the surface, the ground shock, together with the expanding cavity, causes the surface of the ground to mound. Characteristic mound heights at time of venting are also dependent on burial depth, medium, and type of explosive. Mound growth provides a long-period contribution to the waveform between arrival of the GSI pulse and the peak of the gas-venting pulse. This contribution cannot be separated from the other pulses.

THEORY

Charge burial depths for cratering explosions usually are sufficiently deep that strong shocks are not induced in the air, and acoustic approximations suffice. Cole's[33] acoustic approxi-

mation of shock transmission across a water-air interface can be adapted to soil if shear in the ground is ignored:

$$\frac{\Delta p_a}{\Delta p_s} = \frac{2\rho_a c_a \cos \theta_s}{\rho_a c_a \cos \theta_s + \rho_s c_s \cos \theta_a} \tag{3}$$

where subscripts refer to soil or air, Δp is overpressure, ρ is density, c is the sonic velocity, and θ is the angle between the advancing shock front and the surface. Cole's expression is applicable only to the initial peak overpressures in the air at the interface.

If shear in the ground is not to be ignored, an expression[34] for the vertical velocity (u_v) induced by the compression wave of unit amplitude incident upon the free surface is

$$\frac{1}{2} u_{vfs} = \frac{\sin \theta}{\cos 2\phi \tan \theta + 2 \sin^2 \phi \tan 2\phi} \tag{4}$$

where

$$\frac{\sin \theta}{\sin \phi} = \frac{\varepsilon}{\eta} \tag{5}$$

and θ and ϕ are their angles of incidence, and where ε and η are velocities of compression and shear waves, respectively. Reference 34 presents a table of values of the denominator of Equation 4 for a range of values of Poisson's ratio.

From Equations 1, 2, and 4, u_{vfs} can be described as a function of distance from the epicenter and u_{vofs} the vertical velocity at the epicenter. The vertical component of velocity at the epicenter u_{vofs} can be measured or computed from shock strength incident at the surface. The vertical component of the free surface velocity can be set equal to the corresponding velocity in the air above the free boundary to derive the pressure induced in the air; i.e.

$$\Delta p = \frac{7 P_o u_{vfs}}{5 c_a} \tag{6}$$

where P_o is the ambient air pressure. GSI overpressure away from the epicenter can be determined by assuming the pressure profile varies with distance from the epicenter as the particle velocity profile varies with distance. Refinements have been devised[35,36] to take into account both dissipation at the shock front in air, and divergence and crossfeed at the shock front. Crossfeed results from not having all parts of the front at the same strength.

Using an acoustic approximation and a simple source model, Montan[37] has related GSI peak overpressure in the far field (where distance is much larger than the radius of the source) to that at the source as a function of charge burial and distance to the point

of observation. Montan also considers gas-venting pressure produced by cavity pressure where cavity pressures at vent time are estimated from two-dimensional hydrodynamic calculations.

DATA

It is the objective of this paper to use available data as a basis for empirical models that can be used for estimating airblast. Such models can be used for estimating by those who do not have access to relatively expensive, elaborate hydrodynamic calculations. Empirical models are presented for GSI peak overpressure, gas-venting peak overpressure, and positive-phase impulse. Other purposes are to summarize work on close-in airblast from buried explosions and to compare Montan's acoustic model with measured overpressures.

Overpressures, impulses, and durations for most of the events listed in Tables 1 through 5 were available on IBM cards. All values were corrected to standard sea-level conditions (P_o = 14.7 psi; T_o = 15°C). Measurements made over a period of 20 years involved several instrument systems, but the slow rise of pressure waveforms from buried explosions make instrument response an insignificant limitation on data quality, with the possible exceptions of surface bursts or the very shallowest charge burials. Measurements on the Sandia I series were recorded on Brush paper tape recorders and are below the quality of other measurements. Results from that series, however, enter into the data analysis only rarely. Otherwise, the quality of records was good and improved with time.

ANALYSIS

The data have been analyzed by examining separately (a) the GSI peak overpressure, (b) the peak overpressure from venting gas, and (c) the positive-phase impulse. In determining rates of attenuation with distance, power-law least-square fits have been used because neither the quality nor quantity of the data justifies the refinement of a higher-order fit.

Thus, for any given event, $\Delta p = r^{-m}$.

Rate of Attenuation of Airblast with Distance

Spherical attenuation of shock overpressure with distance might be assumed to be nearly r^{-1} as the acoustic region is approached, but theoretical treatments are inconsistent in this regard.

IBM Problem M[38] was not carried to the infinitesimal acoustic limit but in the region from 0.4 to 1 psi the peak overpressure

followed an attenuation rate of about $r^{-1.2}$. (A subsequent recalculation by Whitaker[39] gave $r^{-1.12}$ for overpressure levels of 0.01 to 0.02 psi). Positive-phase impulse followed an attenuation rate of $r^{-0.9}$.

The Kirkwood-Brinkley free-airburst curves for cast TNT[40] were carried only to about the 1-psi level. The region from 1 to 3 psi followed an attenuation rate of $r^{-1.35}$. The positive-phase impulse over the same region shows an attenuation rate of r^{-1}. A recent hydrocode calculation[41] carried to 0.0001639 psi shows an attenuation rate of $r^{-1.0575}$ over the last distance increment of the calculation. Note that this overpressure corresponds to a scaled distance of 84,000 ft/lb$^{1/3}$. For the overpressure range of interest here, average attenuation rates of $r^{-1.22}$ were calculated for the 0.1 to 1.0 psi range, and of $r^{-1.126}$ for the 0.01 to 0.1 range. Thus, even in the spherical free-air case, there are differences between the attenuation rates of various models.

Experimental results from hemispherical surface-burst HE tests[42] indicate that for the region from 0.01 to 0.1 psi the peak overpressure follows an attenuation rate of about $r^{-1.35}$. Positive-phase impulse follows $r^{-1.4}$ approximately.[43]

Examination of the attenuation rates of the three parameters described below will make it clear that a great deal of variation occurs on experiments and that there are only a few consistencies to be found.

Attenuation rates greater than r^{-1} can occur if (a) winds blow toward ground zero from the end of the blast line, and/or (b) a temperature gradient exists, with warmer temperatures at ground level.

Attenuation rates would be less than r^{-1} if (a) winds blow toward the end of the blast line from ground zero; (b) temperature inversions exist, with the ground colder than the air above it; (c) gas-venting peak overpressures are less at closer distances where the wave must diffract down the surface of the mound through which gases vent; (d) waves starting with rounded peaks shock up with propagation over the distance range of the measurements, and/or (e) the size of the source (especially in the case of GSI peak overpressure from buried explosions) relative to the radius to the point of measurement may be important except at very large distances.

Information was not available for most HE events on winds, temperature gradients, or inversions, so those effects cannot be evaluated.

Impulse-HE -- Figure 2 shows m_I for experiments at several scaled burst depths in seven media where

$$I = c\, r^{-m_I}. \qquad (7)$$

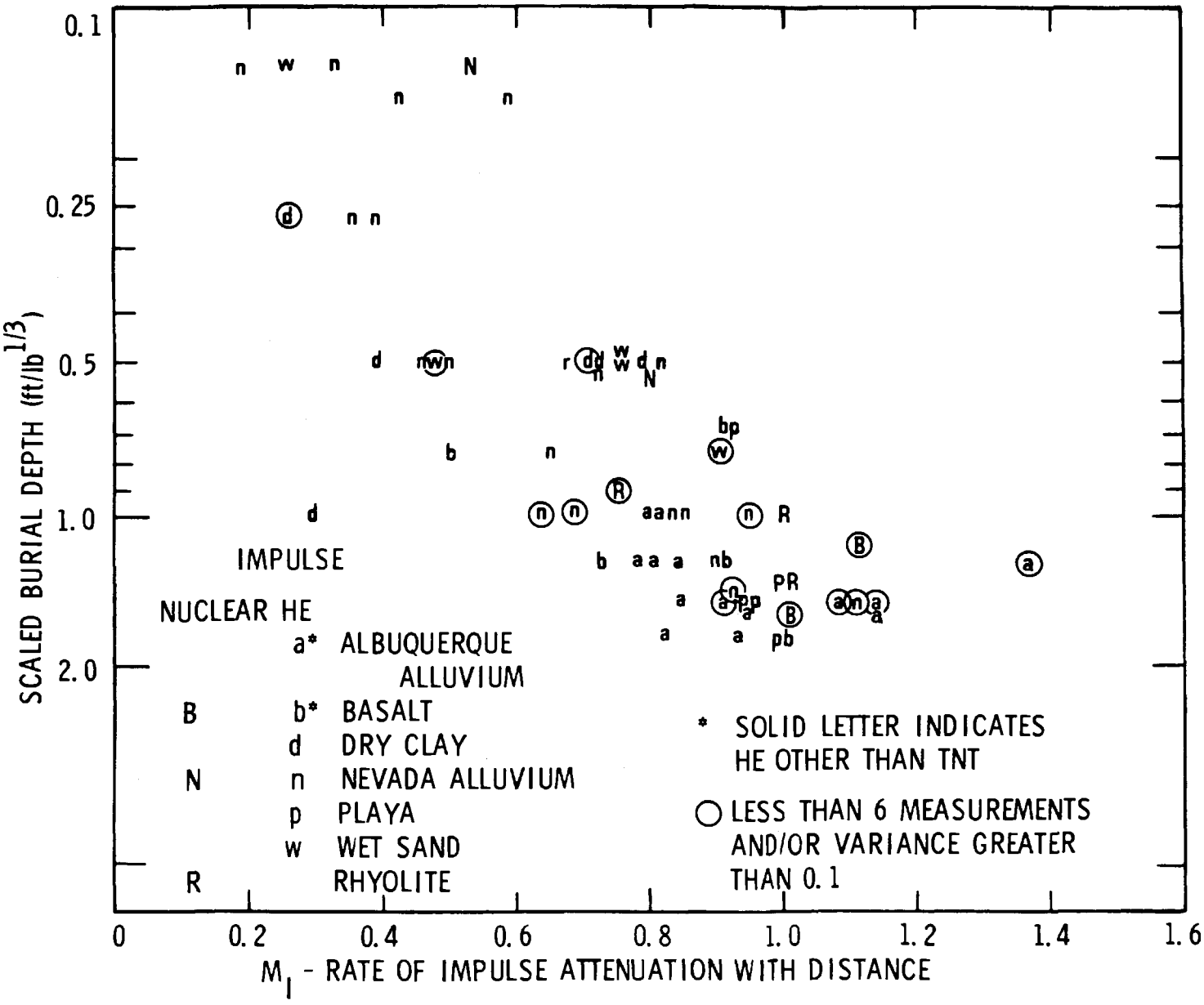

Fig. 2—Rate of attenuation of positive-phase impulse vs scaled charge burial depth.

There is no consistent dependence of m_I on medium. The HE shots in playa and Albuquerque alluvium were fired under especially calm winds and were of a limited range of burial depth; those data show little variation in m_I. Shots in dry clay and NTS alluvium were fired under less ideal wind conditions and spanned a larger range of charge burial depths; those shots show greater variation in m_I. When charge burial depth is considered (Figure 2), a clear dependency of m_I on charge burial depth emerges. The reduction in m_I from theoretical spherical attenuation (r^{-1}) as the surface is approached could be due to a preferential upward direction of airblast as the surface is approached. Under this condition, close gages receive less than for spherical attenuation, and the distant gages more, as blast flows downward along the blast front from upper regions to the ground. Over the burial depth range 0.15 to 2.0 ft/lb$^{1/3}$, the dependence of m_I scaled burial depth can be approximated within the accuracy indicated by the spread of data in Figure 2 by

$$m_I = \frac{\log_{10} \frac{DOB/W^{1/3}}{0.055}}{1.5} \qquad (8)$$

The figure includes data from one shot in basalt with nitromethane, three shots in Albuquerque alluvium where nitromethane was used, and one shot in Albuquerque alluvium with Composition B. With one exception, m_I for those five shots falls within the spread of data from nuclear and TNT shots.

Impulse-NE -- Impulse data for nuclear shots are limited to two shots in basalt (Danny Boy and Sulky), two in NTS alluvium (Jangle U and Teapot ESS) and three shots in rhyolite (Palanquin, Cabriolet and Schooner). The values of m_I for nuclear shots fall within the spread of values for shots in which chemical explosives were used. Although the data are sparse, they tend to confirm the trend shown by data from HE shots of decreasing m_I as the ground surface is approached.

Peak Overpressure-HE and NE -- There is no similar trend in reduction of attenuation rate with decreased burial depth for either gas venting or GSI peak overpressures (Figures 3 and 4). For the latter, there are no data for the shallow burial depths where the GSI pulse is overtaken by the stronger gas-venting pulse. Values of m_p for GSI peak overpressure were spread about the 1.0 to 1.25 region with four exceptions. Four of five nuclear shots have attenuation rates for GSI peak overpressure very close to 1.2.

Values of m_p for gas-venting peak overpressure show a greater scatter, and the center of the spread is decidedly lower than in the case of the GSI peak overpressure. Values for four of five nuclear shots fall in the region of 0.95 to 1.0.

In view of the scatter in values of m, a word is in order concerning variance. Variance is small for shots in which the number of measurements is relatively large; it is small also where special care was taken in gage calibration and where quality of

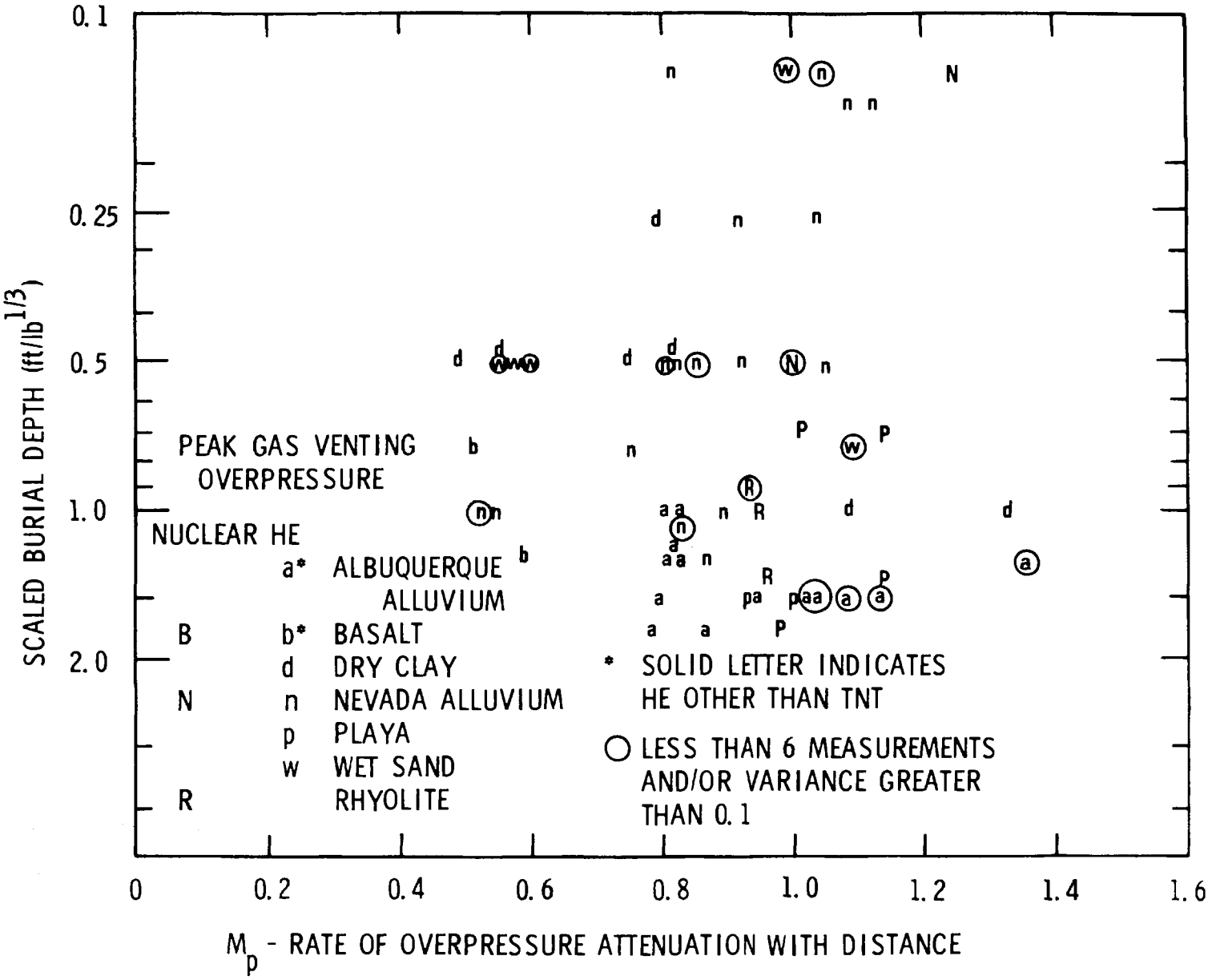

Fig. 3 — Rate of attenuation of ground-shock-induced peak overpressure vs scaled charge burial depth.

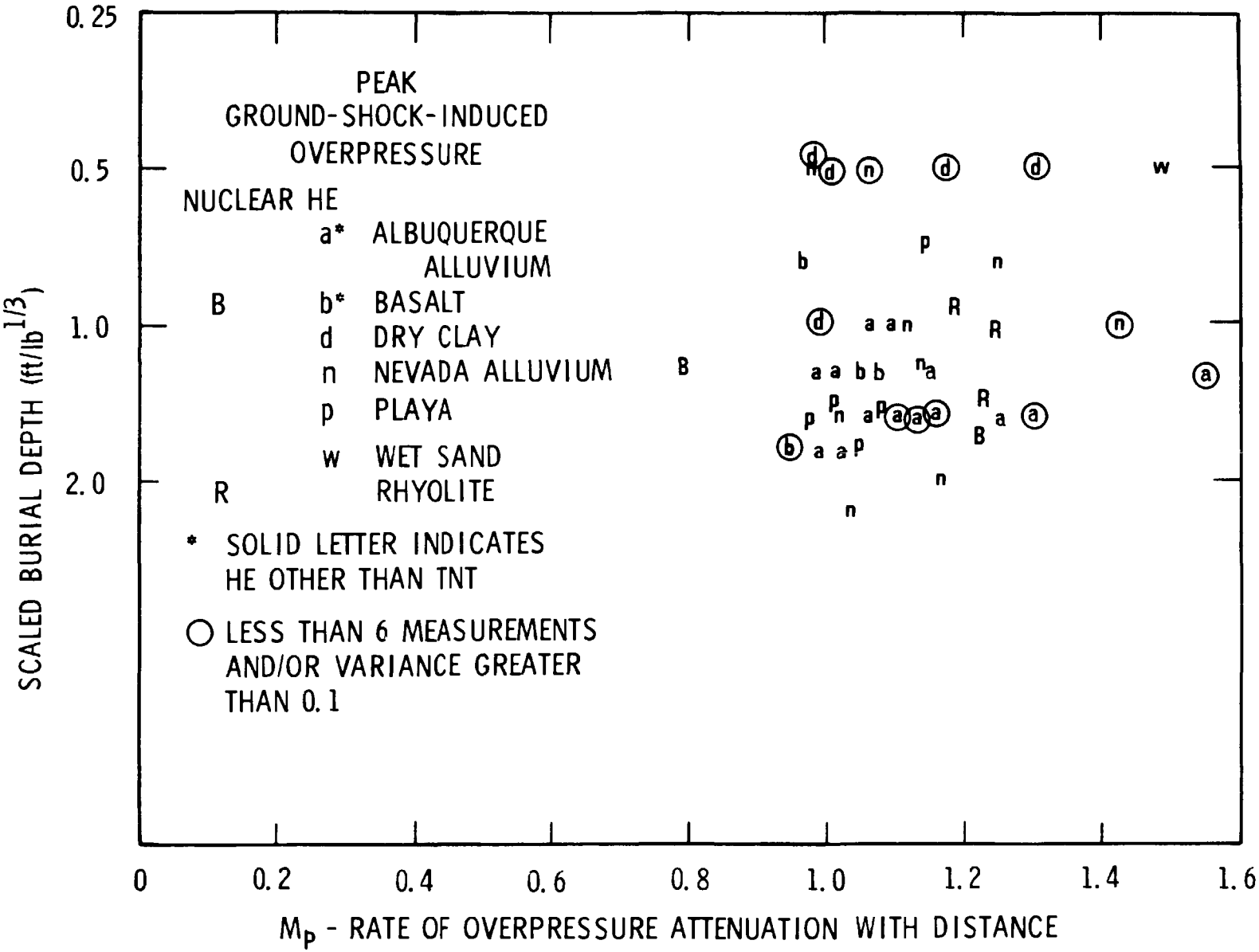

Fig. 4—Rate of attenuation of gas-venting peak overpressure vs scaled charge burial depth.

instrumentation was high; recent measurements, for example, show less variance than early measurements. Where variance was high or low for one blast parameter, it usually was the same for the other two parameters. This reflects the quality of the measurements on a particular shot or series. The following list is a generalization of the variance observed.

Medium	Small variance (±)	Large variance (±)
HE		
Albuquerque alluvium	CAPSA 10 (0.04-0.045)	CAPSA 11-13 (0.09-0.17)[a]
	CAPSA 1-9 (0.02-0.06)	Sandia III (not determinable)
Basalt	Buckboard & Pre-schooner II (0.02-0.07)	
Dry clay		UET (0.06-0.12)
		Mole 100 series (0.05-0.19)
NTS alluvium	Scooter, Stagecoach (0.02-0.06)	Sandia I (not determinable)
		Mole 200 (0.06-0.13)
		Mole 400 (0.04-0.15)
		Jangle HE (0.03-0.09)
Playa	211 Series (0.015-0.06)	
Wet sand		Mole 300 (0.03-0.2)
NE	Jangle U (0.03-0.06)	Teapot ESS (0.04-0.2)
	Cabriolet (0.02-0.05)	Danny Boy (0.90-0.36)
	Schooner (0.06-0.07)	Sulky (0.21-0.42)
		Palanquin (0.06-0.12)

[a]These were nitromethane or Composition B shots with values of m usually well over 1.0.

It is worth noting that the fact that the variances of m are as small as 0.02 for shots in several media indicates that first-order fit to measured data is quite adequate and lends credence to the argument that much of the variation has to do with quality of measurement.

Rate of Suppression of Airblast with Charge Burial

HE Experiments -- Airblast is attenuated (suppressed) also by charge burial. Analysis done in connection with the Cabriolet event[25] suggested that, within the accuracy of the data, airblast suppression at a constant scaled range could be expressed by

$$\Delta p = k \left(\frac{DOB}{W^{1/3}}\right)^{-n} \qquad (9)$$

A custom has evolved in which charge burial depths have been chosen such that scaled burial depth increases by specified increments. The scaled burial depths most frequently used are:

0.13 ft/lb$^{1/3}$ (Top of TNT sphere tangent to ground surface)
0.25
0.50
0.75
1.00
1.25
1.50

This custom led to the distribution of charge burial depths illustrated in Figure 5 for gas-venting peak overpressure at a scaled distance of 5 ft/lb$^{1/3}$ for HE shots in NTS desert alluvium. The data points represent values given at 5 ft/lb$^{1/3}$ by equations of the type of Equation 7 for each shot. As indicated in Figure 5, it appeared that in the case of gas-venting peak overpressure (and also for positive-phase impulse) there were two separate rates of airblast attenuation--one rate for shots shallower than 0.5 ft/lb$^{1/3}$ and one for deeper shots. In three of the six media (NTS alluvium, dry clay, and wet sand) for which there are HE data spanning both ranges of scaled burial depth, there were similar suggestions of differences in attenuation rates. Further analysis has shown that airblast suppression may be represented better by semi-log presentation than by log-log presentation, and moreover that the two-slope characteristic of Figure 5 results from a combination of the customary burial depths and the log-log presentation. Thus, a better expression for blast suppression with charge burial is

$$I, \Delta p = \frac{k}{10 \exp\left[n\left(\frac{DOB}{W^{1/3}}\right)\right]} \qquad (10)$$

Using equations for airblast ($I, \Delta p$) versus distance for each shot, values of k and n (Equation 10) were determined for all HE shots in six media at scaled ranges of 5, 7, 10, 20, and 50 ft/lb$^{1/3}$. In no case were data extrapolated beyond the scaled distance at which measurements were made, although, if the variance in rate of attenuation with distance was small, little error would be involved in doing so. As a result, there are less data for 20 ft/lb$^{1/3}$, and still less for 50 ft/lb$^{1/3}$. Accordingly, variance of k and n is always larger for 20 ft/lb$^{1/3}$ than for closer ranges, and is even larger for 50 ft/lb$^{1/3}$.

Airblast suppression at a single scaled range (7 ft/lb$^{1/3}$) for HE shots in six media is illustrated for impulse (Figure 6), gas venting peak overpressure (Figure 7) and GSI peak overpressure (Figure 8). Points plotted in each figure represent a value for a constant scaled range from a calculated airblast-distance relationship (Equation 7) for each shot. For each medium and scaled

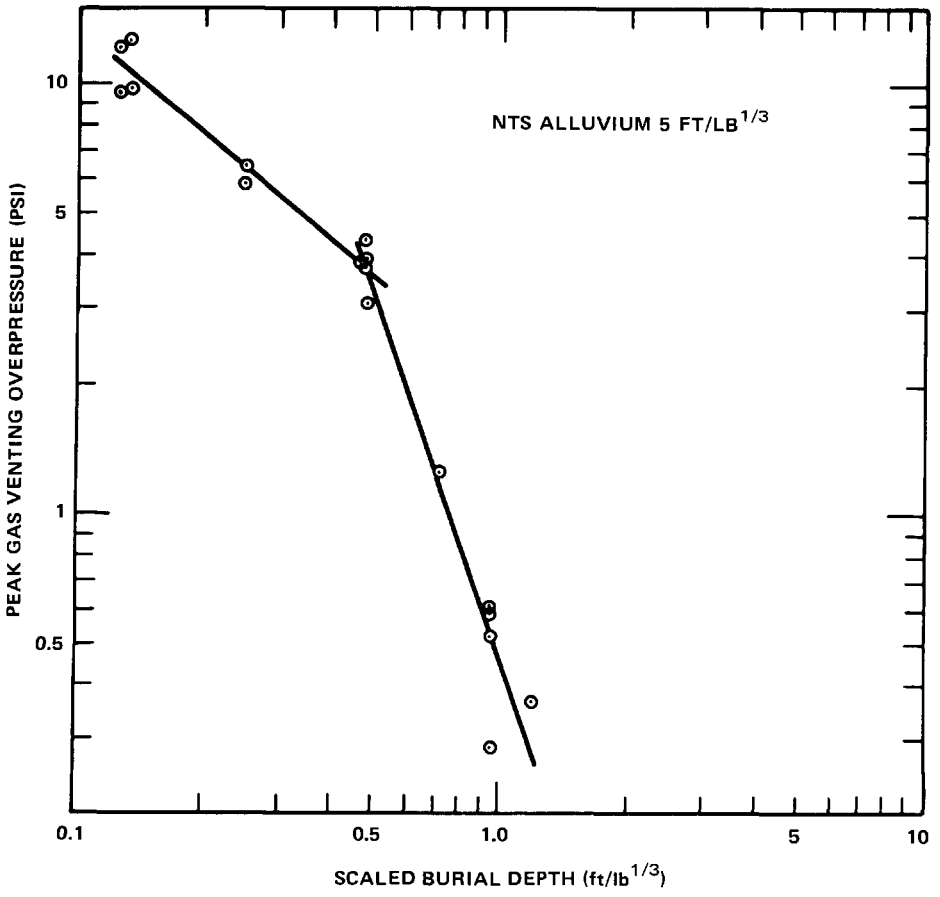

Fig. 5 — Peak gas-venting overpressure vs scaled charge burial depth.

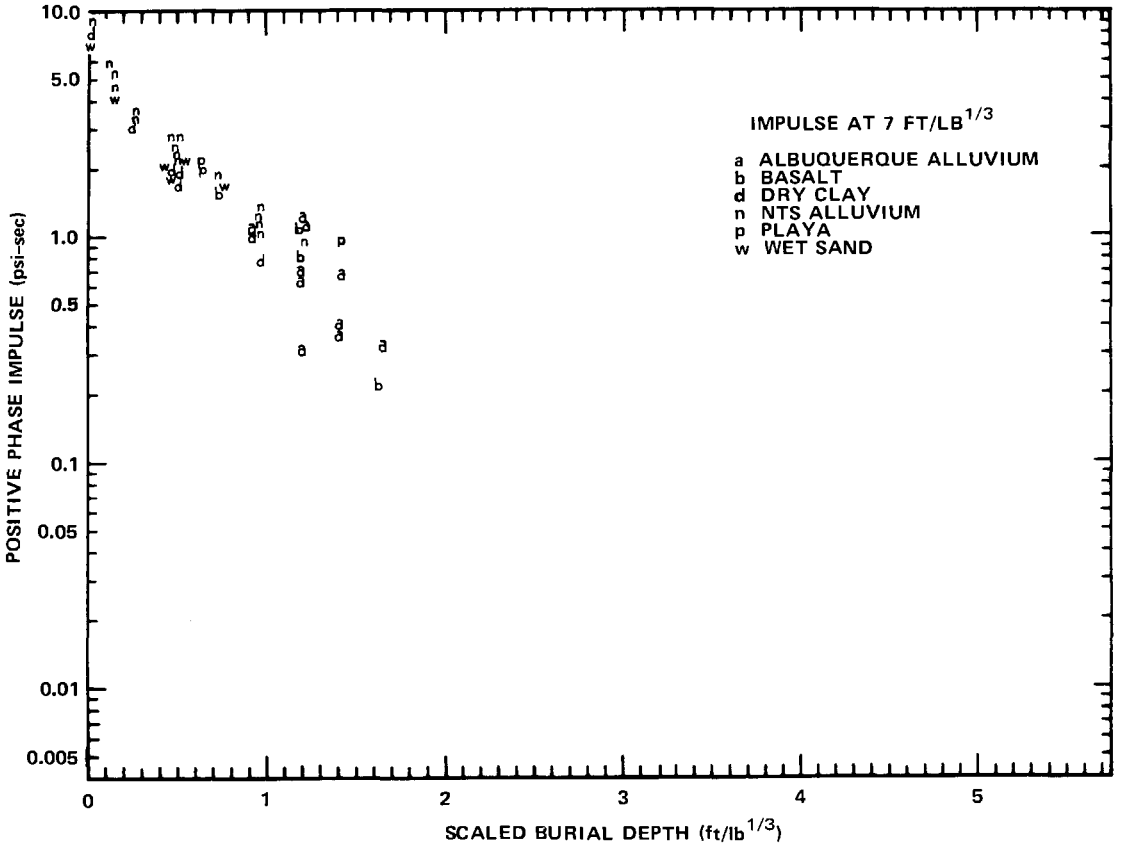

Fig. 6 — Positive-phase impulse data vs scaled charge burial depth for six media.

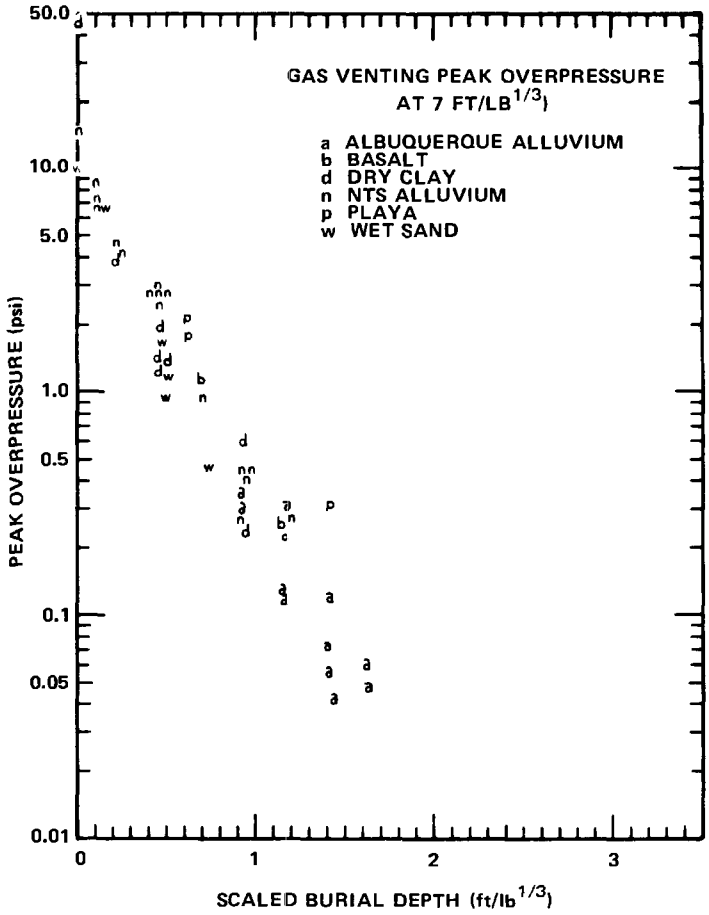

Fig. 7—Gas-venting peak overpressure data vs scaled charge burial depth for six media.

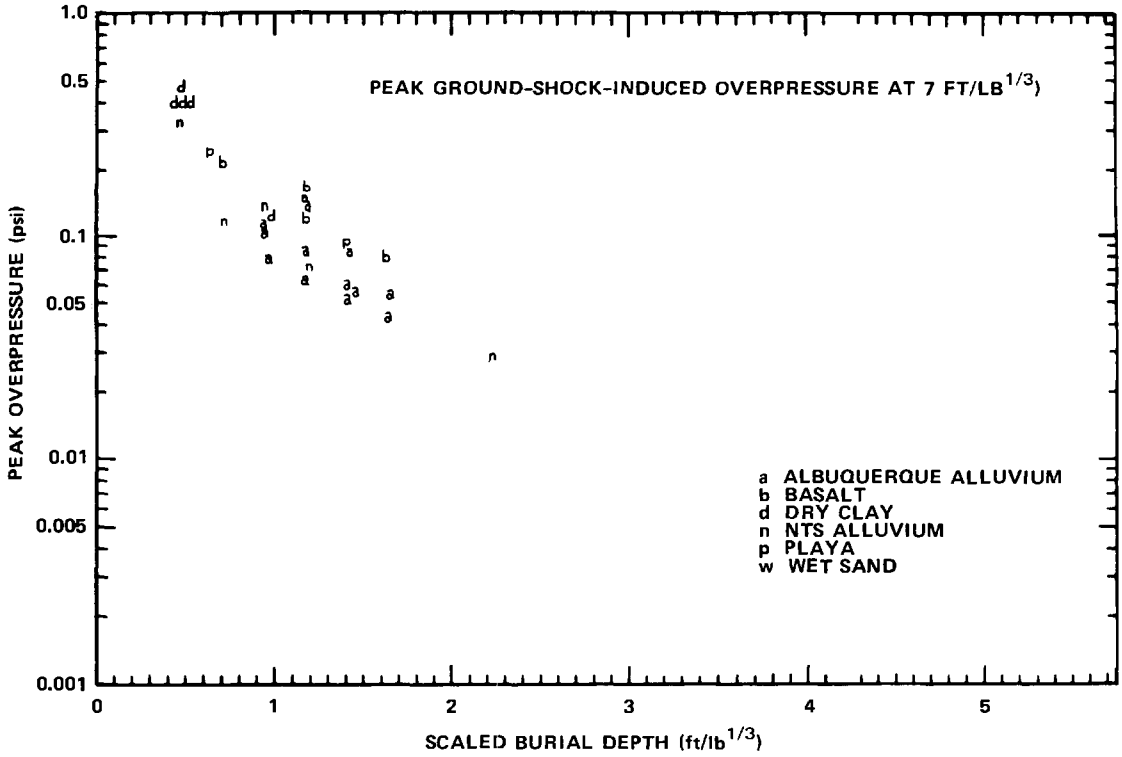

Fig. 8—Peak ground-shock-induced overpressure data vs scaled charge burial depth for six media.

distance, suppression expressions (Equation 10) were determined. Examining the expressions (Table 6) shows that n is either constant or exhibits a slight dependence on scaled range. The dependence may be a result of too few shots in a given medium. The constant k always shows a dependence on scaled range

$$k = c'r^{-m'} \tag{11}$$

where m' constitutes a synthesized rate of attenuation with distance of the blast parameter for a given medium (so long as n is constant for that medium).

Table 6 lists the equations for each medium and each parameter, developed from fits to data of Figures 6 through 8. Results of these fits are illustrated in Figures 9 through 11 for a single scaled range (7 $ft/lb^{1/3}$). Using the equations of Table 6 it is possible to predict any of the three parameters of airblast from buried HE shots over the depth of burst and distance spans of the data for any of the six media within the accuracy of the measured parameters.

An attempt was made to correlate k and n or c' and m' with known physical characteristics of the media, either singly or in combination. The attempt was completely unsuccessful. Nonetheless, if predictions are necessary for explosions in media for which there are no data, one alternative is to use that one of the six for which results are presented here, that qualitatively compares best with the medium under consideration. Another alternative is to use the last expression in Table 6, which was obtained using all data without regard for medium.

Nuclear Events - Adequate expressions for airblast as a function of distance cannot be developed for all of the nuclear cratering events for any of the blast parameters. There was no measured GSI pulse for the Jangle U, Teapot ESS, or Sedan events. Gas-venting pulses were not measurable for the Sulky and Danny Boy events. These pulses, of course, were non-existent for the contained nuclear explosions (Table 5). The number of measurements on contained events other than Dumont and Greely was small, and airblast-distance relationships must be used cautiously. Accordingly, a spread is used for contained nuclear events in Figures 9 through 11.

The nuclear events are few, and are spread over four media (alluvium, basalt, rhyolite, and tuff), preventing development of meaningful relationships for airblast suppression with charge burial. Consequently, a different means is used here for presenting blast suppression as a function of burial depth, and for comparing suppression for nuclear events with that for HE shots. In Figures 9 through 11 blast suppression versus burial depth for each of the three airblast parameters at a scaled distance of 7 $ft/lb^{1/3}$ is presented. Nuclear data are presented separately for each event.

TABLE 6

Equations for Airblast Predictions

	Ground-Shock-Induced Peak Overpressure (psi)	Gas Venting Peak Overpressure (psi)	Positive Phase Impulse (psi-sec)
Albuquerque Alluvium - TNT	$\Delta P = \frac{2.5\left(\frac{r}{W^{1/3}}\right)^{-1.1}}{10\exp\left[0.5\left(\frac{DOB}{W^{1/3}}\right)\right]}$ (c)	$\Delta P = \frac{13\left(\frac{r}{W^{1/3}}\right)^{-0.74}}{10\exp\left[1.15\left(\frac{DOB}{W^{1/3}}\right)\right]}$ (c)	$I = \frac{20\left(\frac{r}{W^{1/3}}\right)^{-0.65}}{10\exp\left[0.8\left(\frac{DOB}{W^{1/3}}\right)\right]}$ (a)
NTS Alluvium	$\Delta P = \frac{8.5\left(\frac{r}{W^{1/3}}\right)^{-1.6}}{10\exp\left[0.58\left(\frac{DOB}{W^{1/3}}\right)\right]}$	$\Delta P = \frac{110\left(\frac{r}{W^{1/3}}\right)^{-1.13}}{10\exp\left[2\left(\frac{r}{W^{1/3}}\right)^{-0.15}\left(\frac{DOB}{W^{1/3}}\right)\right]}$	$I = \frac{13.5\left(\frac{r}{W^{1/3}}\right)^{-0.38}}{10\exp\left[0.38\left(\frac{r}{W^{1/3}}\right)^{0.3}\left(\frac{DOB}{W^{1/3}}\right)\right]}$ (a)
Basalt	$\Delta P = \frac{3.5\left(\frac{r}{W^{1/3}}\right)^{-1.03}}{10\exp\left[0.47\left(\frac{DOB}{W^{1/3}}\right)\right]}$ (a)	$\Delta P = \frac{23\left(\frac{r}{W^{1/3}}\right)^{-0.39}}{10\exp\left[1.4\left(\frac{DOB}{W^{1/3}}\right)\right]}$ (a)	$I = \frac{11\left(\frac{r}{W^{1/3}}\right)^{-0.12}}{10\exp\left[0.54\left(\frac{r}{W^{1/3}}\right)^{0.28}\left(\frac{DOB}{W^{1/3}}\right)\right]}$ (a)
Albuquerque Alluvium - Other Than TNT	$\Delta P = \frac{900\left(\frac{r}{W^{1/3}}\right)^{-1.59}}{10\exp\left[1.25\left(\frac{DOB}{W^{1/3}}\right)\right]}$ (b)	$\Delta P = \frac{950\left(\frac{r}{W^{1/3}}\right)^{-0.93}}{10\exp\left[2.35\left(\frac{DOB}{W^{1/3}}\right)\right]}$ (b)	$I = \frac{720\left(\frac{r}{W^{1/3}}\right)^{-1.08}}{10\exp\left[1.65\left(\frac{DOB}{W^{1/3}}\right)\right]}$ (b)
Dry Clay	$\Delta P = \frac{20\left(\frac{r}{W^{1/3}}\right)^{-1.32}}{10\exp\left[1.2\left(\frac{DOB}{W^{1/3}}\right)\right]}$ (a)	$\Delta P = \frac{24\left(\frac{r}{W^{1/3}}\right)^{-0.17}}{10\exp\left[1.3\left(\frac{r}{W^{1/3}}\right)^{0.2}\left(\frac{DOB}{W^{1/3}}\right)\right]}$ (a)	$I = \frac{12\left(\frac{r}{W^{1/3}}\right)^{-0.34}}{10\exp\left[0.7\left(\frac{r}{W^{1/3}}\right)^{0.21}\left(\frac{DOB}{W^{1/3}}\right)\right]}$ (a)
Wet Sand	No data	$\Delta P = \frac{135\left(\frac{r}{W^{1/3}}\right)^{-1.33}}{10\exp\left[3.1\left(\frac{r}{W^{1/3}}\right)^{-0.27}\left(\frac{DOB}{W^{1/3}}\right)\right]}$ (a)	$I = \frac{20\left(\frac{r}{W^{1/3}}\right)^{-0.63}}{10\exp\left[0.72\left(\frac{r}{W^{1/3}}\right)^{0.11}\left(\frac{DOB}{W^{1/3}}\right)\right]}$ (a)
Playa	$\Delta P = \frac{5.6\left(\frac{r}{W^{1/3}}\right)^{-1.2}}{10\exp\left[0.54\left(\frac{DOB}{W^{1/3}}\right)\right]}$ (d)	$\Delta P = \frac{80\left(\frac{r}{W^{1/3}}\right)^{-1.13}}{10\exp\left[1.01\left(\frac{DOB}{W^{1/3}}\right)\right]}$ (d)	$I = \frac{23\left(\frac{r}{W^{1/3}}\right)^{-0.89}}{10\exp\left[0.46\left(\frac{DOB}{W^{1/3}}\right)\right]}$ (d)
	$\Delta P = \frac{3.5\left(\frac{r}{W^{1/3}}\right)^{-0.93}}{10\exp\left[0.59\left(\frac{DOB}{W^{1/3}}\right)\right]}$ (e)	$\Delta P = \frac{160\left(\frac{r}{W^{1/3}}\right)^{-1.15}}{10\exp\left[1.3\left(\frac{DOB}{W^{1/3}}\right)\right]}$ (e)	$I = \frac{27\left(\frac{r}{W^{1/3}}\right)^{-0.88}}{10\exp\left[0.58\left(\frac{DOB}{W^{1/3}}\right)\right]}$ (e)
All Media	$\Delta P = \frac{5\left(\frac{r}{W^{1/3}}\right)^{-1.05}}{10\exp\left[0.6\left(\frac{DOB}{W^{1/3}}\right)\right]}$ (b)	$\Delta P = \frac{70\left(\frac{r}{W^{1/3}}\right)^{-0.93}}{10\exp\left[1.5\left(\frac{DOB}{W^{1/3}}\right)\right]}$ (b)	$I = \frac{15\left(\frac{r}{W^{1/3}}\right)^{-0.5}}{10\exp\left[0.56\left(\frac{r}{W^{1/3}}\right)^{0.17}\left(\frac{DOB}{W^{1/3}}\right)\right]}$ (c)

$$\Delta P = \frac{c'\left(\frac{r}{W^{1/3}}\right)^{-m'}}{10\exp\left[n\left(\frac{DOB}{W^{1/3}}\right)\right]}$$

NOTES: (a) Valid for r = 5 to 10 ft/lb$^{1/3}$
(b) Valid for r = 5 to 20 ft/lb$^{1/3}$
(c) Valid for r = 5 to 50 ft/lb$^{1/3}$
(d) Valid for r = 7 to 10 ft/lb$^{1/3}$
(e) Valid for r = 20 to 50 ft/lb$^{1/3}$

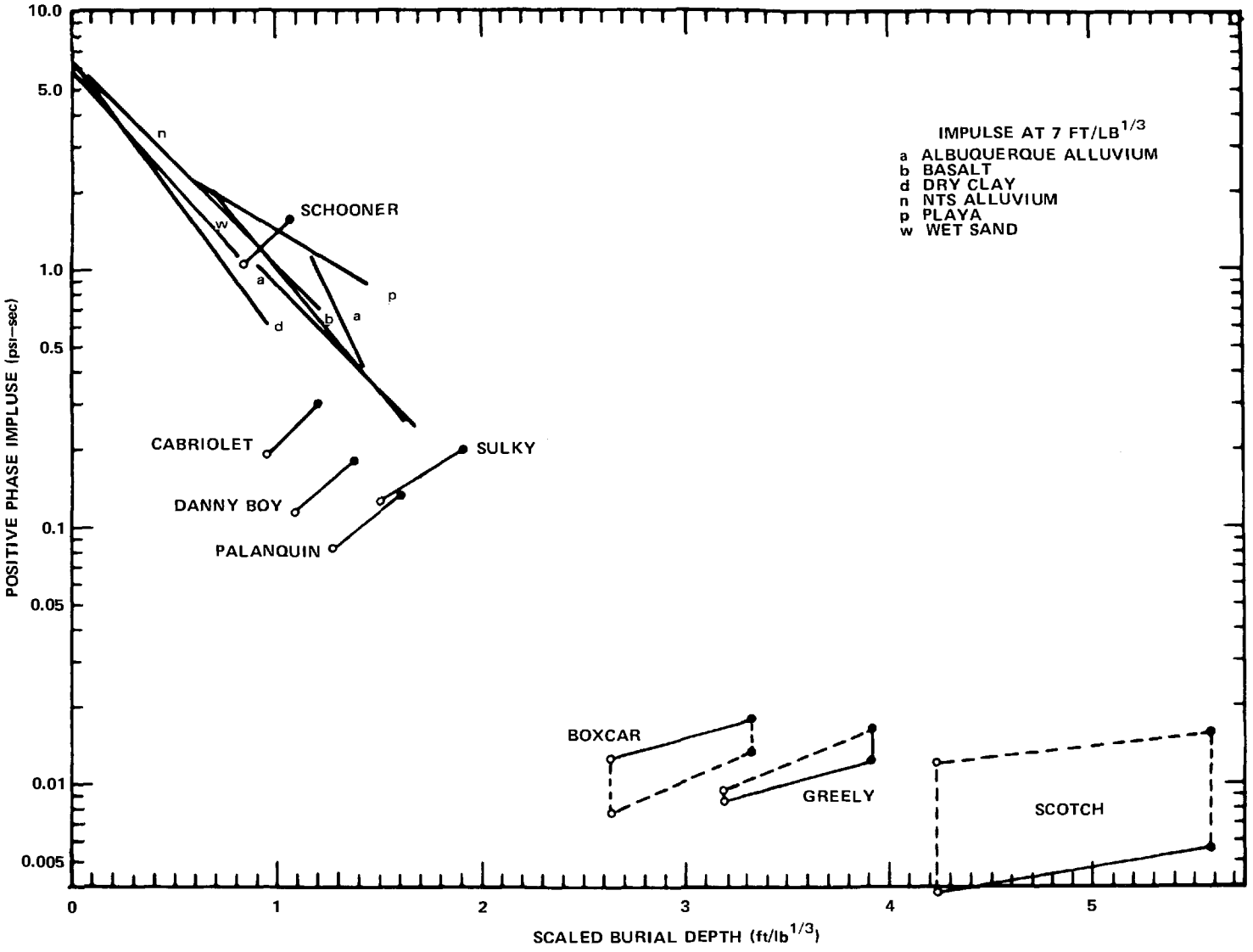

Fig. 9—Impulse vs scaled charge burial depth; HE relationships compared with nuclear data.

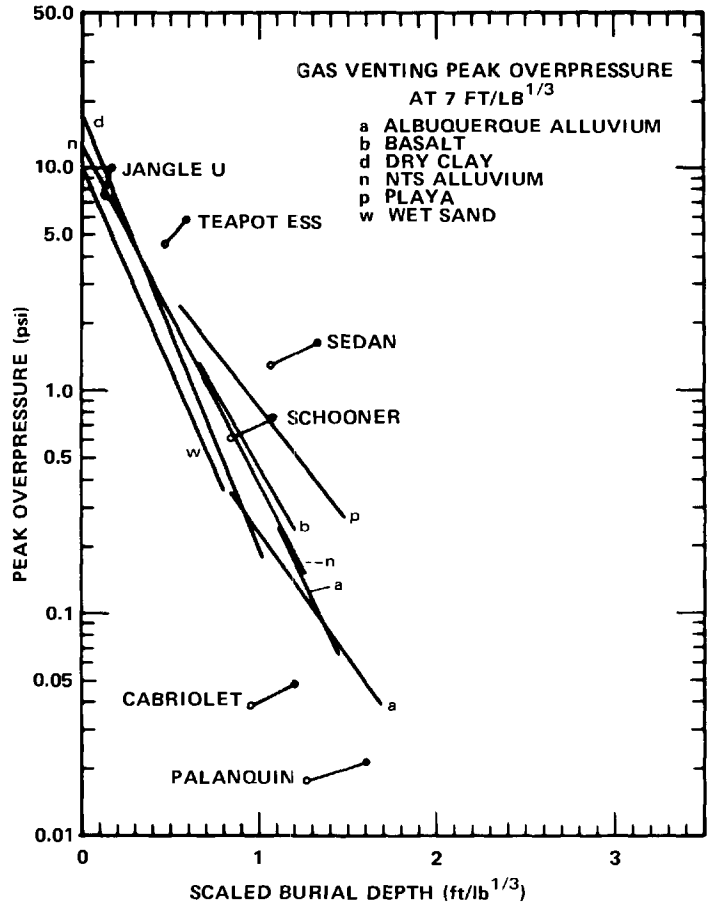

Fig. 10 — Gas-venting peak overpressure vs scaled charge burial depth; HE relationships compared with nuclear data.

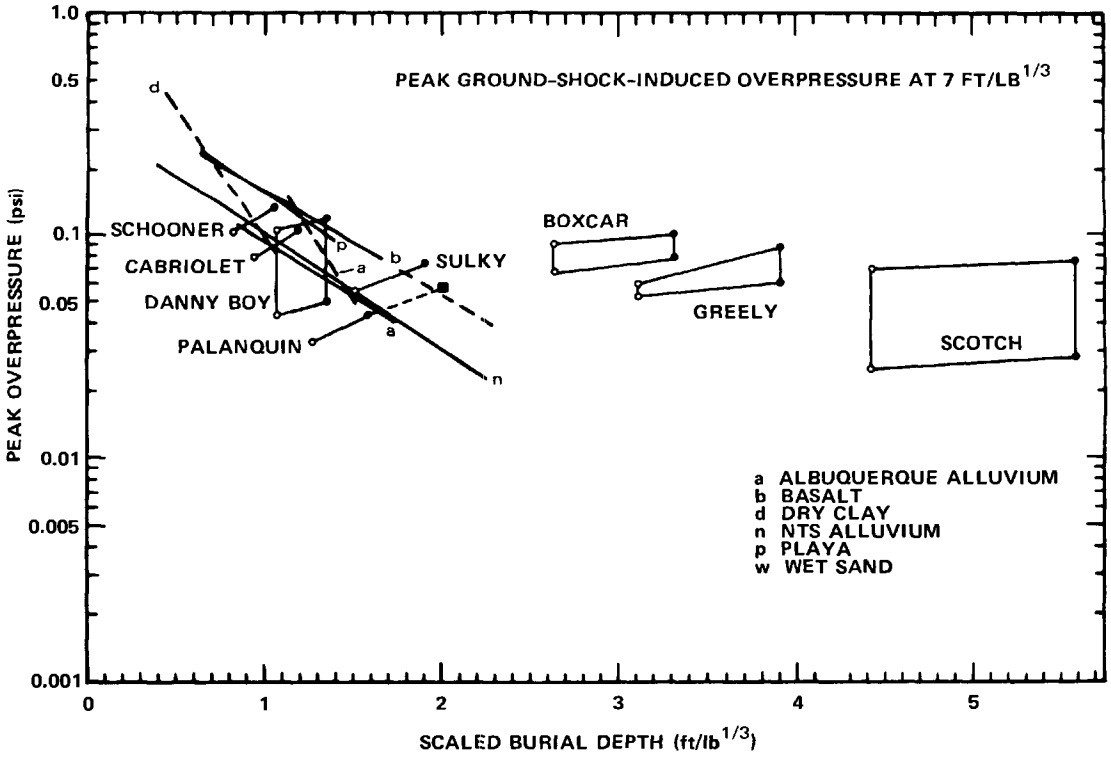

Fig. 11 — Peak ground-shock-induced overpressure vs scaled charge burial depth; HE relationships compared with nuclear data.

Scaling - Cube-root scaling, i.e., linear dimensions and times for two events proportional to the cube roots of their charge weights, has been applied throughout the foregoing to HE events. No indication of any departure from cube root scaling is suggested by any of the HE data. For above-ground explosions, airblast measurements on nuclear explosions agree with measurements from TNT explosions only if the nuclear explosion is considered to have a TNT equivalent energy yield of half its nominal yield.*

While there is no a priori reason to expect the same equivalence for buried explosions,** the opportunity to examine the possibility has been provided in Figures 9 through 11 by presenting each airblast parameter scaled to one pound TNT equivalent on the basis of both the nominal yield (the open circles) and one-half the nominal yield (filled circles).

The positive-phase impulse from nuclear shots shows a continuation from HE data of decrease with increased burial depth (Figure 9). The trend is reasonably uniform even though impulse from Boxcar, Greely, Scotch, Danny Boy, and Sulky is entirely from the GSI pulse while that from Palanquin, Cabriolet, and Schooner is from both the GSI and gas-venting pulses--as is impulse from the HE shots. There is no consistent clue to nuclear-HE equivalence.

Peak gas-venting overpressure (Figure 10) shows the decrease in overpressure with increased burial depth for the HE shots. Nuclear events in alluvium (Teapot ESS and Sedan) produced gas-venting overpressures greater than in HE shots, while two of the cratering events in rhyolite (Cabriolet and Palanquin) produced less. The Schooner event produces about the same as would be expected from HE shots. This attests to the greater dependence of gas-venting peak overpressure on medium (and especially its moisture content) in the case of the nuclear events than in the HE shots. It attests further to a consequent inapplicability of HE shots as a source of predicting gas-venting peak overpressure from nuclear events.

Suppression with burial depth of GSI peak overpressure (Figure 11) presents a different picture. No GSI pulse is observed for burial depths shallower than about 0.5 $ft/lb^{1/3}$. From four of the nuclear cratering shots there is consistently better agreement with HE basalt data on the basis of one-half nominal yield. Palanquin would have to have a nominal yield of 2 kt to agree with the other four events. It is this observation for

---

*The equivalence actually varies with overpressure, but is close to half for most of the overpressure range from which it has been derived. Recent calculations[41] suggest an equivalence of 0.7 for the lower overpressure range for free-air explosions.

**Nuclear energy is deposited locally, and afterburning of HE gases is less (if, in fact, afterburn exists at all for buried explosions).

these five nuclear cratering shots that is taken as evidence that the nuclear-HE equivalence observed for airblast from above-ground explosions is also applicable to that from cratering explosions. This observation is possible only for the GSI peak overpressure, where medium and moisture content effects are not an overriding factor.

GSI peak overpressure from contained explosions, either separately or together with the cratering nuclear explosions, appears to follow a law of blast suppression with charge burial depth quite different from that of the HE shots. The suggestion is that GSI airblast from contained nuclear explosions is suppressed less effectively by charge burial. Data from HE shots at comparable burial depths are not available to show whether this is a characteristic of nuclear shots only. The larger area source of the GSI pulse from contained nuclear explosions may be a possible explanation.

Comparison with Montan's Acoustic Approximation

Montan has shown[37] that ground surface motion can be described by

$$\frac{U_{vfs}}{U_{ovfs}} = \left(\frac{DOB}{S}\right)^{n_m} \tag{12}$$

where S is slant range. He shows further that overpressure as a function of horizontal range (r) would have the form

$$\frac{\Delta p}{\Delta P_o} = \alpha\left(\frac{r}{DOB}\right)^{-\mu} \tag{13}$$

Values for n_m of about 3 for alluvium and rhyolite and about 6 for hard rock were found from experiment results, corresponding to α of 0.318 and 0.188 respectively. The latter were evaluated for four HE shots in alluvium, as well as for three HE shots and two NE shots in basalt.

The availability of pressure data from a larger number of shots permits similar evaluations to be made easily. These questions were asked:

1. Is the exponent μ precisely -1; if not, what is it?
2. What are values of α for $\mu = -1$, and for the exponent evaluated from the data?

Of course, $\mu = m$ (m from Eq. 7) for the GSI pulse and μ departs from 1 for precisely the same reasons that m departs from 1 (see Figure 3). Since the departure is biased on the higher side, the acoustic approximation departs from reality accordingly.

Tables 7 and 8 list values for μ and α indicated by the data, and α indicated by the data where μ is held equal to 1 according to an acoustic assumption. Values of n_m are listed also, derived from α.

One unique feature of the HE data of Table 7 is the large values of α (low n_m) for the Albuquerque alluvium, a feature that carries over into some shots in NTS alluvium. Alluvial soils appear as nearly elastic media since for elastic media $n_m = 2$ (Ref. 44). Large values of α can be attributed to either a unique characteristic of the medium or to a measurement which failed to record a Δp_o as large as actually occurred (in the case of the CAPSA series); in the case of NTS alluvium Δp_o was not measured in any instance, but was calculated (using Equation 6 and ambient conditions) from a surface zero velocity versus depth of burst relationship or from measured surface zero velocity.

Several shots were used to evaluate the acoustic theory further. Two of the better of these are shown in Figure 12 (Scooter) and Figure 13 (Cabriolet). Note that for Scooter there are four separate values shown for α and n_m:

1. From n_m derived from measured surface motion data,
   $\alpha = 0.252\text{-}0.268$
   $n_m = 3.65\text{-}3.95$

2. From Reference 37, $\alpha = 0.318$
   $n_m = 3.00$

3. From measured pressure data, $\left(\frac{r}{DOB}\right)^{1.147}$, $\alpha = 0.381$
   $n_m = 2.55$

4. From measured pressure data, $\left(\frac{r}{DOB}\right)^{-1}$, $\alpha = 0.286$
   $n_m = 3.35$

These observations can be made: (1) none of the four approaches departs appreciably from measured data; (2) the acoustic (r^{-1}) attenuation, although approximate, is not realistic; (3) the range of both α and n_m exhibited does not depart appreciably from the data, and (4) failure to account for actual rates of attenuation is as important as uncertainties or variations of ±25 percent or more in α or n_m.

Similar observations can be made concerning Cabriolet (Figure 10). Similar comparisons were made for other shots, resulting in these additional observations: (1) uncertainties or variations in measured surface velocity profiles often detract from the accuracy of n_m and hence the utility of acoustic theory, and (2) Δp_o derived from measured surface velocity or surface velocity relationships can also introduce variations or uncertainty in evaluation of the acoustic approximation.

TABLE 7

Single HE Shots

			μ	α	n_m	$\mu = 1$ α	$\mu = 1$ n_m
			NTS Desert Alluvium				
Jangle HE	3	c	0.978	0.517	<2.0	0.541	<2.0
Mole 402		c	1.248	0.462	2.15	0.288	3.35
404		c	1.423	0.605	<2.0	0.305	3.15
Sandia I	-9	c	1.142	0.272	3.55	0.205	5.30
Stagecoach	1	b	1.038	0.285	3.35	0.277	3.50
	2	b	1.063	0.502	2.00	0.435	2.30
	3	b	1.114	0.536	<2.00	0.400	2.45
Scooter		b	1.147	0.381	2.55	0.286	3.35
All NTS Alluvium							
			Albuquerque Alluvium				
Sandia III	-1	d	1.104	0.543	<2.0	0.432	2.30
Sandia III	-2	d	1.150	0.729	<2.0	0.523	<2.0
Capsa	1	a	1.133	0.633	<2.0	0.489	2.05
	2	a	0.986	0.467	2.15	0.480	2.10
	3	a	1.091	0.883	<2.0	0.714	<2.0
	4	a	1.021	0.548	<2.0	0.528	<2.0
	5	a	1.063	0.649	<2.0	0.607	<2.0
	6	a	0.987	0.430	2.30	0.442	2.25
	7	a	1.065	0.674	<2.0	0.565	<2.0
	9	a	1.011	0.404	2.40	0.395	2.50
	10	a	1.115	1.033	<2.0	0.810	<2.0
	11	a	1.238	0.599	<2.0	0.376	2.55
	12	a	1.550	0.492	2.05	1.318	<2.0
	13	a	1.300	0.979	<2.0	0.594	<2.0
			Basalt				
Buckboard	11	b	0.961	0.218	4.80	0.237	4.25
	12	b	1.050	0.278	3.50	0.257	3.85
	13	b	0.943	0.238	4.25	0.259	3.80
			Rhyolite				
Pre-Schooner II		a	1.076	0.456	2.20	0.401	2.45
			Playa				
TTR 211-4		b	0.973	0.397	2.45	0.436	2.30
TTR 211-7			1.073	0.461	2.20	0.422	2.35

a - P_o measured

b - P_o derived from measured surface velocity and ambient conditions

c - P_o derived from relation for surface velocity versus DOB and ambient conditions for HE shots

d - P_o assumed same as measured for other shots in same medium at same scaled burial depth

TABLE 8

Contained Nuclear Shots
and Nuclear Cratering Shots

					$\mu = 1$	
		μ	α	n^1	α	n_m
Dumont	a	1.137	0.475 to 0.746	<2.0 to 2.10	0.381 to 0.60	<2.0 to 2.55
Greely	a	1.143	0.341	2.80	0.299	3.20
			Basalt			
Danny Boy	b	0.785	0.201	5.45	0.292	3.30
Sulky	b	1.220	0.393	2.50	0.243	4.15
			Rhyolite			
Palanquin	a	1.236	0.349	2.75	0.231	4.45
Cabriolet	a	1.240	0.511	<2.0	0.314	3.05
Schooner	a	1.203	0.328	2.90	0.219	4.75

a - P_o measured

b - P_o derived from relation for surface velocity versus DOB and ambient conditions using yield of nuclear shot 1 kt = 10^6 lb HE

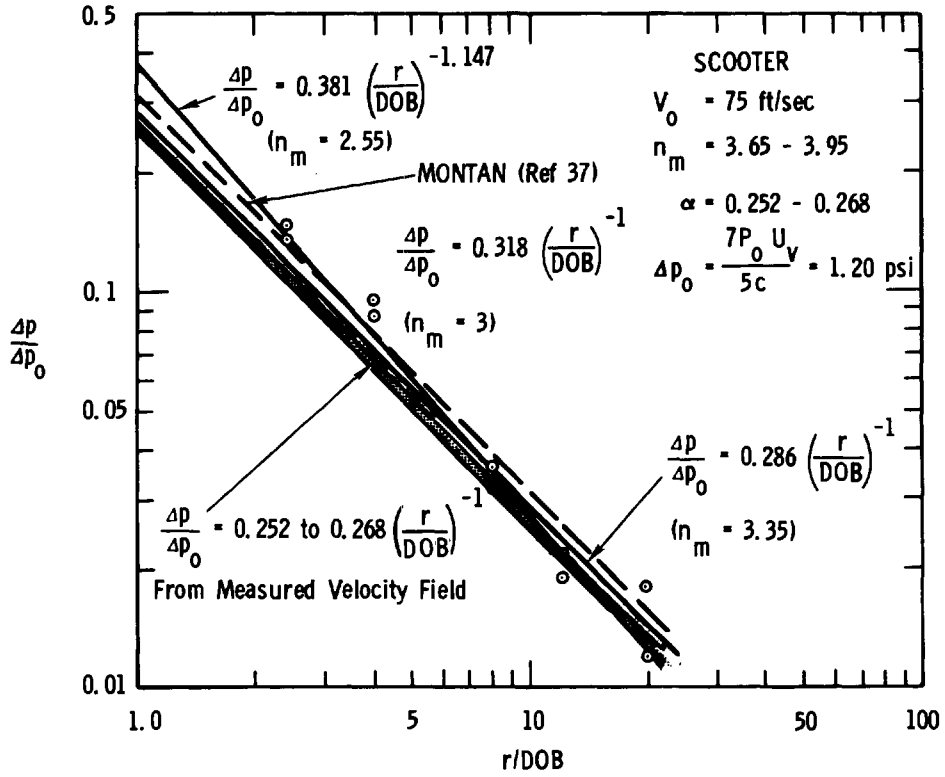

Fig. 12—Comparison of acoustic approximation with Scooter measurements.

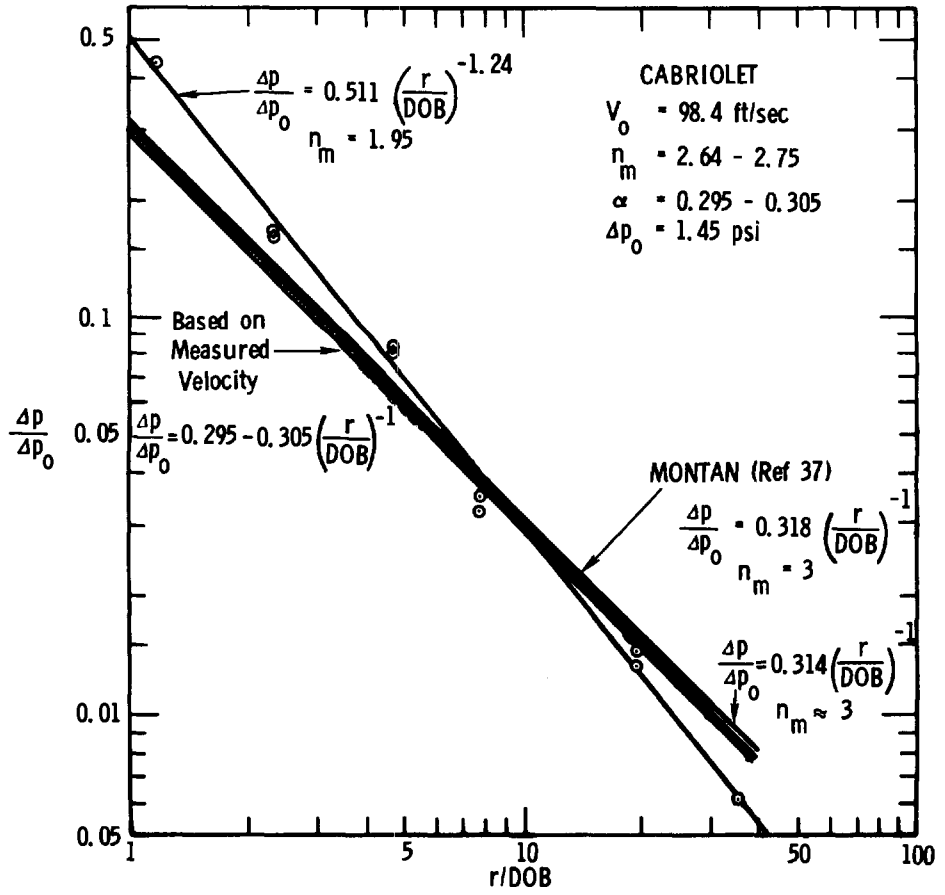

Fig. 13—Comparison of acoustic approximation with Cabriolet measurements.

Figure 3 showed that attenuation rates observed on experiments averaged well above r^{-1}. While there are almost certainly some meteorological effects contributory to the scatter, it is difficult to see how shot conditions could have been chosen to provide the bias illustrated by the figure. This, together with calculated attenuation rates, suggests that while the acoustic case may be approximated, it is not achieved precisely.

Rows and Arrays

Airblast parameters from row charges were found to approximately equal N^{α} times the same parameter for a single charge, where N is the number of charges. The power α was different for each parameter; it was a function of charge spacing, and increased as spacing between charges in the row decreased. The power was always greater perpendicular to the row (but always less than 1) than off the end of the row.

Pressure and impulse were always greater perpendicular to the row than off the end of the row, and the difference increased as the number of charges increased. The increase was also a function of charge spacing. The shots listed in Table 2 suggest that there also are medium dependencies, but the data are too sparse to suggest their nature. Rates of airblast attenuation with distance for row charges exhibited about the same variation for each parameter and from one parameter to another as did single charges.

Similar variations were observed also for quincuncial (symmetrical five-charge) arrays. There GSI peak overpressures were about 2.25 and 1.7 times those of a single charge at the same burial depth for 10- and 16-ft. spacing respectively. Corresponding ratios for gas-venting peak overpressures were reversed, i.e., 1.7 and 2.25 times respectively. For positive-phase impulse, the ratio was 3.3 for both spacings. GSI peak overpressures were in agreement with those to be expected perpendicular to a row of five such charges. Gas-venting peak overpressures from the array were larger by comparison.

CONCLUSIONS

Rate of attenuation of airblast with distance is affected by local meteorology and gage performance. There is no consistent dependence of attenuation rate on medium. Attenuation rates are different for GSI peak overpressures, gas-venting peak overpressure, and positive-phase impulse. The latter is the only parameter in which a clear dependence of attenuation rate on scaled burial depth is demonstrated.

It has been possible, using the high-explosive data, to provide relationships with which to predict any of three components of airblast from the buried HE shots. The relationships are, of course, applicable only for the media from which data were

obtained, only over the range of charge burial depth in those media, and over the range of distances from the charges at which measurements were made. The accuracy of the prediction is comparable to scatter in the measured airblast parameter. No GSI overpressures were observed for explosions where the charge burial depth was less than 0.50 ft/lb$^{1/3}$.

In the case of nuclear explosions the number of events is too small, considering medium effects, to permit derivation of similar relationships. Gas-venting peak overpressures for the Teapot ESS and Sedan nuclear cratering explosions in NTS alluvium were larger than would be predicted from HE shots; that of the Schooner event in rhyolite was about equal, whereas the remaining events in basalt or rhyolite had peak gas-venting pressures lower than would be predicted from results of chemical explosions. This stresses the importance of the medium, and particularly its moisture, in the determination of gas-venting peak overpressure.

Impulses from nuclear explosions are generally comparable with those from chemical explosions and continue the trend of blast suppression with charge burial established by the chemical explosions.

The GSI peak overpressures for completely contained explosions decrease less rapidly with increased charge burial depth than is indicated by the HE data. For the nuclear cratering explosions, the peak GSI overpressures are in better agreement with results from chemical explosions if the nuclear explosions are considered to have a TNT energy equivalence equal to half their nominal yield. This makes equivalence for underground nuclear events agree with the equivalence observed for above-ground explosions.

Availability of data from a large number of chemical and nuclear explosions has permitted a comparison of experiment results with Montan's acoustic approximation. His acoustic prediction is generally comparable with measured overpressures. The most obvious departure from the acoustic approximation occurs because the rate of overpressure attenuation with distances is greater than the r^{-1} predicted by acoustic theory. It was found that a major source of uncertainty in applying acoustic theory results from uncertainties or inaccuracies in measurement of the ground surface velocity profile.

ACKNOWLEDGMENTS

This work was supported by the Division of Peaceful Nuclear Explosives, U. S. Atomic Energy Commission. The author recognizes the cooperation of the Dikewood Corporation in providing airblast data cards, and of J. W. Long in programming all computations.

REFERENCES

1. Vaile, R. B., Jr., Surface Structure Program, Underground Explosion Tests At Dugway, AFSWP-298, Stanford Research Institute, Menlo Park, California, March 1952

2. Doll, E. B., High Explosive Tests, Operation Jangle, WT-365, Armed Forces Special Weapons Project, October-November 1951

3. Sachs, D. C. and L. M. Swift, Small Explosion Tests, Project MOLE, Vols. I and II, AFSWP-291, Stanford Research Institute, Menlo Park, California, December, 1955

4. Murphey, B. F. and E. S. Ames, Air Pressure Versus Depth of Burst, SC-TM-42-59(51), Sandia Laboratories, Albuquerque, New Mexico, February 1959

5. Murphey, B. F., High Explosive Crater Studies: Tuff, SC-4574(RR), Sandia Laboratories, Albuquerque, New Mexico, April 1961

6. Vortman, L. J., et al, 20-Ton HE Cratering Experiment in Desert Alluvium, Project STAGECOACH, SC-4596(RR), Sandia Laboratories, Albuquerque, New Mexico, May 1962

7. Vortman, L. J., et al, 20-Ton and 1/2-Ton High Explosive Cratering Experiments in Basalt Rock, Project BUCKBOARD, SC-4675(RR), Sandia Laboratories, Albuquerque, New Mexico, November 1960

8. Perret, W. R., et al, Project SCOOTER Final Report, SC-4602(RR), Sandia Laboratories, Albuquerque, New Mexico, October 1963

9. Vortman, L. J., Airblast and Craters from Rows of Two to Twenty-five Charges, SC-RR-68-655, Sandia Laboratories, Albuquerque, New Mexico, January 1969

10. Unpublished data, Sandia Laboratories, Albuquerque, New Mexico

11. Reed, J. W. and L. J. Vortman, Airblast Measurements, Project PRE-SCHOONER II, PNE-512F, Sandia Laboratories, Albuquerque, New Mexico, February 1968

12. Unpublished data, Sandia Laboratories, Albuquerque, New Mexico and U. S. Corps of Engineers, Nuclear Cratering Group, Livermore, California

13. Vortman, L. J., Close-in Airblast From a Row Charge in Basalt, PNE-608F, Sandia Laboratories, Albuquerque, New Mexico, August 4, 1965

14. Vortman, L. J., Comparison of Airblast from Two Sizes of Row Charges, SC-RR-66-415, Sandia Laboratories, Albuquerque, New Mexico, October 1966

15. Keefer, J. M., W. F. Jackson, and D. P. Lefevre, "Close-in Air Blast from a Row of Buried Charges," Ballistic Research Laboratories, Aberdeen Proving Ground, Maryland, Chapter in Project Pre-Gondola II, Summary Report, U. S. Corps of Engineers, Nuclear Cratering Group, Livermore, California, to be published

16. Rappleyea, C. Annette, Crater, Ejecta, and Air-Blast Studies from Five High-Explosive Charges in a Horizontal Square Array, SC-RR-66-480, Sandia Laboratories, Albuquerque, New Mexico, April 1967

17. Vortman, L. J., "Close-in Airblast Measurements," Sandia Laboratories, Albuquerque, New Mexico, Chapter in Project Pre-Gondola III, Phase I, Summary Report, PNE-1114, U. S. Corps of Engineers, Nuclear Cratering Group, Livermore, California, to be published

18. Gannon, W. F., et al, Blast and Shock Measurements II, Operation Jangle, WT-367, Armed Forces Special Weapons Project, Washington, D. C., October-November 1951

19. Sachs, D. C. and L. M. Swift, Underground Explosion Effects, Operation Teapot, Project 1.7, WT-1106, Armed Forces Special Weapons Project, Washington, D. C., March 3, 1958

20. Vortman, L. J., Close-in Airblast from a Nuclear Detonation in Basalt, Project DANNY BOY, POR-1810, Sandia Laboratories, Albuquerque, New Mexico, June 1962

21. Vortman, L. J., Close-in Airblast from a Nuclear Event in NTS Desert Alluvium, Project SEDAN, PNE-211F, Sandia Laboratories, Albuquerque, New Mexico, October 2, 1964

22. Keefer, J. H., Free-air and Free-field Blast Phenomena from a Small Yield Device, Operation Sunbeam, Shot Johnie Boy, POR-2280, Ballistic Research Laboratory, Aberdeen Proving Ground, Aberdeen, Maryland, November 27, 1963

23. Vortman, L. J., Close-in Air Blast from a Relatively Deep Low-Yield Nuclear Detonation in Basalt, Project SULKY, PNE-711F, Sandia Laboratories, Albuquerque, New Mexico, May 1965

24. Vortman, L. J., Close-in Air Blast from a Cratering Nuclear Detonation in Rhyolite, Project Palanquin, PNE-902F, Sandia Laboratories, Albuquerque, New Mexico, April 1966

25. Vortman, L. J., Close-in Air Blast from the Cabriolet Event, PNE-951, Sandia Laboratories, Albuquerque, New Mexico, October 25, 1968

26. Vortman, L. J., Close-in Airblast from the Buggy I Event, PNE-320, Sandia Laboratories, Albuquerque, New Mexico, to be published

27. Vortman, L. J., Close-in Airblast from the Schooner Event, PNE-521, Sandia Laboratories, Albuquerque, New Mexico, to be published

28. Reed, J. W. and H. W. Church, Microbarograph Measurement, Project Gnome, VUP-2001, Sandia Laboratories, Albuquerque, New Mexico, January 1962

29. Perret, W. R., Personal Communication

30. Reed J. W., Personal Communication

31. Preliminary Report on Effects of Milrow Detonation, Amchitka Island, Alaska, October 2, 1969, Press Release, U. S. Atomic Energy Commission, October 22, 1969

32. Wheeler, V. E. and R. G. Preston, Scaled Free-Field Particle Motions from Underground Nuclear Explosions, UCRL-50563, Lawrence Radiation Laboratory, Livermore, California, August 1, 1968

33. Cole, R. H., Underwater Explosions, Princeton University Press, Princeton, New Jersey, 1948

34. Knopoff, L., R. W. Fredricks, A. F. Gangs, and L. D. Porter, "Surface Amplitudes of Reflected Body Waves," Geophysics, Vol. SSII, No. 4., October 1957, pp. 842-847

35. Merritt, M. L., Airpressures from a Deep Underwater Burst; Operation Wigwam, WT-1035, Sandia Laboratories, Albuquerque, New Mexico, May 1955

36. Merritt, M. L. and C. R. Mehl, Airpressures from Deep Underwater Explosion, II, Crossfeed, SC-TM-274-55 (51), Sandia Laboratories, Albuquerque, New Mexico, December 1955

37. Montan, D. N., "Source of Airblast from the Underground Explosion," Transactions, American Nuclear Society, Vol. II, No. 2, November 1968, pp. 541-542

38. Bethe, H., et al, Blast Wave, LA-2000, Los Alamos Scientific Laboratory, Los Alamos, New Mexico, March 27, 1958

39. Whitaker, W. A., Air Force Weapons Laboratory, Personal Communication

40. Kirkwood, J. G. and S. R. Brinkley, Jr., Theoretical Blast-Wave Curves for Cast TNT, OSRD 5481, NDRL A-341, Office of Scientific Research and Development, Washington 25, D. C., August 23, 1945

41. Lehto, D. L. and R. A. Larson, Long Range Propagation of Spherical Shockwaves from Explosions in Air, NOLTR 69-88, U. S. Naval Ordnance Laboratory, Explosions Research Department, White Oak, Maryland, July 1969

42. Kingery, C. H. and B. F. Pannill, Peak Overpressure versus Scaled Distance for TNT Surface Bursts (Hemispherical Charges), BRL Memorandum Report No. 1518, Ballistic Research Laboratories, Aberdeen Proving Ground, Maryland, April 1964

43. Kingery, C. H., Airblast Parameters versus Distance for Hemispherical TNT Surface Burst, BRL Report 1344, Ballistic Research Laboratories, Aberdeen Proving Ground, Maryland, September 1966

44. Montan, D. N., Personal Communication